

## Optical properties of metallic nanoparticles in Ni-ion-implanted $\alpha$ -Al<sub>2</sub>O<sub>3</sub> single crystals

X. Xiang and X. T. Zu<sup>a)</sup>

*Department of Applied Physics, University of Electronic Science and Technology of China, Chengdu, 610054, People's Republic of China*

S. Zhu and L. M. Wang

*Department of Nuclear Engineering and Radiological Sciences and Department of Materials Science & Engineering, University of Michigan, Ann Arbor, Michigan 48109*

(Received 30 July 2003; accepted 31 October 2003)

64 keV Ni ion implantation was performed at room temperature up to a dose of  $1 \times 10^{17} \text{ cm}^{-2}$  in  $\alpha$ -Al<sub>2</sub>O<sub>3</sub> single crystals. The charge states, structure, and optical properties of metallic embedded Ni nanoparticles were studied by using x-ray photoelectron spectroscopy (XPS), transmission electron microscopy, and optical spectroscopy, respectively. XPS analysis showed that implanted Ni ions are mainly in charge state of metallic Ni<sup>0</sup>. Nanoparticles distributed from the surface to 30 nm below the surface were observed in a high-angle annular dark-field image. The size of nanoparticles ranges from 1 to 5 nm in diameter. A high-resolution electron microscopy image indicated the Ni-implanted area had been entirely amorphized. A new broad absorption band centered at 400 nm appeared in the optical absorption spectrum of the as-implanted crystal, due to surface plasma resonance of Ni nanoparticles. We did not find any emission band in the as-implanted sample under a Xe lamp excitation wavelength of 250–430 nm in a spectrophotometer. © 2004 American Institute of Physics. [DOI: 10.1063/1.1636817]

Ion implantation has become a versatile and powerful technique for forming nanoparticles. It shows potential promise as a means of modifying the near-surface mechanical, electrical, optical, and magnetic properties in insulator matrices, due to quantum confinement effects.<sup>1</sup> Ion implantation has been used to produce metallic nanoclusters embedded in a ceramic matrix for three decades.<sup>2</sup> Many researches are concentrated on optical properties of silica glass, and metallic nanocrystals formed by ion implantation, including Au, Ag, Ga, and other transition metal elements.<sup>3–5</sup>

Single crystal  $\alpha$ -Al<sub>2</sub>O<sub>3</sub> (sapphire) has been often used in microelectronics for photoelectric devices or as window materials. Some metallic nanocrystals, such as Au, Al, Fe, Y, Ag, formed by ion implantation have been studied in Al<sub>2</sub>O<sub>3</sub> host crystals.<sup>6–9</sup> There are no reports on metallic Ni nanoparticles formation induced by ion implantation in Al<sub>2</sub>O<sub>3</sub> single crystals. In this letter, the charge states, structure and optical properties of metallic Ni nanoparticles in Ni-implanted Al<sub>2</sub>O<sub>3</sub> crystals were studied by using x-ray photoelectron spectroscopy (XPS), transmission electron microscopy (TEM), and optical spectroscopy, respectively.

The colorless, transparent synthetic single crystals  $\alpha$ -Al<sub>2</sub>O<sub>3</sub> were cut perpendicularly to the  $\langle 0001 \rangle$  axis,  $10 \times 15 \times 1 \text{ mm}^3$  in size. The samples were optically polished to a mirror-like finish before ion implantation. The Ni ion implantation in Al<sub>2</sub>O<sub>3</sub> was performed at an energy of 64 keV with dose of  $1 \times 10^{17} \text{ cm}^{-2}$  in a vacuum chamber of  $1.8 \times 10^{-3} \text{ Pa}$ . The samples were kept at room temperature with the circulation of cooling water during ion implantation. The ion beam current density was under  $0.5 \mu\text{A}/\text{cm}^2$  to avoid heating the samples. The samples were tilted off-axis by

around 7° to avoid channeling implantation. After implantation, all the crystals turned gray and the transparency decreased.

X-ray photoelectron spectra of as-implanted samples were obtained at room temperature with a KRATOS X SAM 800 x-ray photoelectron spectrometer with monochromatic Al K<sub>α</sub> ( $h\nu = 1486 \text{ eV}$ ). The Ar<sup>+</sup> ion beam etching of the samples was conducted at an energy of 3 keV and a current density of  $10 \mu\text{A}/\text{cm}^2$ . The etching rate was approximately 1 nm/min. A JEOL2010F scanning transmission electron microscopy (STEM)/TEM analytical electron microscope operating at 200 keV was used for bright-field, high-angle annular dark-field (HAADF) and high-resolution electron microscopy (HREM) imaging. The lens conditions were defined for a probe size of 0.2 nm and with a collection angle of 50 mrad for HAADF STEM imaging. Optical absorption measurements in the UV-visible were made in a SHIMADZU UV-2100 spectrophotometer. The wavelength used in the experiment ranged from 200 to 800 nm. Luminescence tests were performed with a Hitachi 850 photoluminescence spectrophotometer, a Xe lamp was the excitation source.

The Ni-implanted samples had been etched 2 nm with Ar<sup>+</sup> ion before XPS measurements in order to remove surface contamination. Figure 1 shows the XPS spectra of Ni 2p<sub>3/2</sub> energy level at etching depth of 2 and 12 nm, respectively. The C 1s peak at 285.0 eV is used to calibrate the spectra. The as-implanted spectra can be resolved into two Gaussian components. The peak at 852.3 eV is attributed to metallic Ni<sup>0</sup>, and the peak at 856.6 eV may be due to Ni<sup>2+</sup> (NiAl<sub>2</sub>O<sub>4</sub>) or Ni<sup>3+</sup> (Ni<sub>2</sub>O<sub>3</sub>). It is clear that the implanted Ni ions are prominent in charge state of metallic Ni<sup>0</sup>. The charge states of Ni have no distinct change with the increas-

<sup>a)</sup>Author to whom correspondence should be addressed; E-mail: zuxt@sohu.com

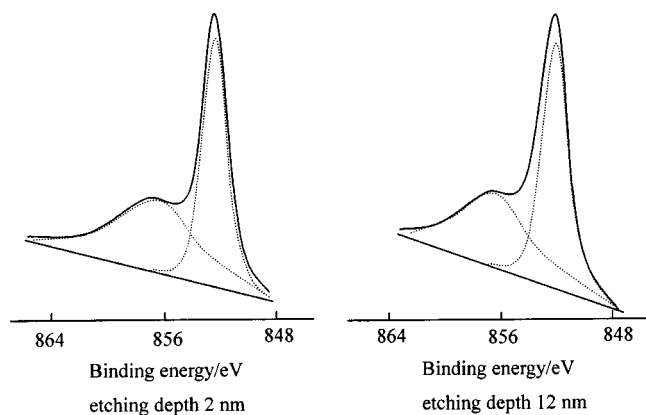


FIG. 1. X-ray photoelectron spectra of Ni  $2p_{3/2}$  energy level of  $\text{Ni}^+$ -implanted  $\text{Al}_2\text{O}_3$  crystals showing implanted Ni ions mainly in charge state of metallic  $\text{Ni}^0$ . The charge states of Ni have no distinct change with the increasing etching depth. Real line-experimental curve, point line-Gaussian simulated curve.

ing etching depth. But the calculation indicates that the Ni concentrations increase from 9.55% to 9.84% with the etching depths increasing from 2 to 12 nm.

Figure 2 shows a bright-field and a HAADF STEM cross-sectional image indicating size and distribution of nanoparticles embedded in  $\text{Al}_2\text{O}_3$  formed by Ni ion implantation. For HAADF STEM imaging, intensity in the image is approaching a  $Z^2$  dependence on atomic number  $Z$ .<sup>10</sup> This suggests a HAADF STEM image provides information on element distribution. In this study, Ni has a much higher  $Z$  than both Al and O, therefore the nanoparticles of Ni show bright contrast. As is shown in Fig. 2, nearly spherical embedded nanoparticles are distributed from the surface to 30 nm below the surface, consistent with calculation results by SRIM 2000 code. The size of nanoparticles ranges from 1 to 5 nm in diameter. Figure 3 is a HREM image showing the crystalline structure of nanoparticles of Ni in the surface of  $\text{Al}_2\text{O}_3$  matrix. The image shows clearly the Ni-ion implanted area is amorphized entirely.

The optical absorption spectra of as-grown and as-implanted  $\text{Al}_2\text{O}_3$  single crystals are shown in Fig. 4. As a comparison, the absorption spectrum of an irradiated crystal with electron beam at the same dose is given. The electron irradiation of the sample was performed at room temperature in air, with electron beam energy 1.6 MeV and current density  $26 \mu\text{A}/\text{cm}^2$ . A very weak absorption band around 225 nm appears in the as-grown matrix. There is a 240–280 nm

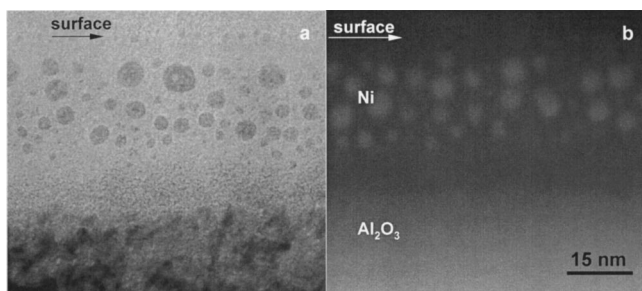


FIG. 2. A bright-field (a) and a HAADF STEM (b) cross-sectional image in the near surface of as-implanted  $\text{Al}_2\text{O}_3$  matrix. Nearly spherical embedded nanoparticles, 1–5 nm in diameter, are distributed from the surface to 30 nm below the surface.

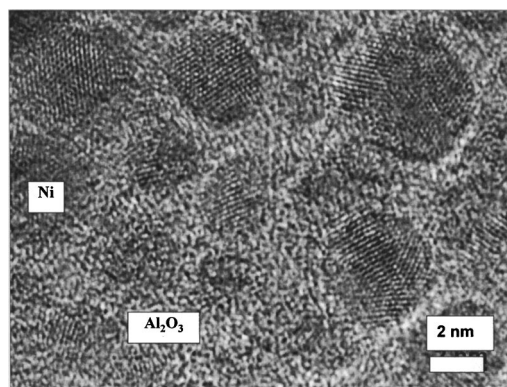


FIG. 3. A HREM image showing structure of Ni nanoparticles in the near surface of  $\text{Al}_2\text{O}_3$  matrix.

band centered at 250 nm in the electron-irradiated sample. However, a broad absorption band peaked at 400 nm can be seen in the Ni-ion implanted  $\text{Al}_2\text{O}_3$  crystal. We did not detect any emission band in the as-implanted sample under a Xe lamp excitation wavelength of 250–430 nm in a spectrophotometer.

Single crystal  $\alpha\text{-Al}_2\text{O}_3$  belongs to the space group  $D_{3d}^6 - R\bar{3}C$  (rhombohedral) with a wide band gap ( $E_g \sim 9 \text{ eV}$ ). Therefore, its intrinsic absorption is in the ultraviolet wave band, and the pure single crystals look colorless and transparent in the visible region. So its absorption spectrum is a smooth line in the visible wave band (Fig. 4). The absorption band around 225 nm corresponds to  $\text{F}^+$  color centers formed by  $\text{O}^{2-}$  vacancy captured single electron.<sup>11</sup> And  $\text{O}^{2-}$  vacancies formed because oxygen atmosphere reduced during crystal growth. However, in the spectrum of electron-irradiated sample, the absorption band shifts to 250 nm corresponding to F color centers. This is due to charge transfer and the equation between  $\text{F}^+$  and F centers is  $\text{F}^+ + e \rightarrow \text{F}$ .<sup>12</sup> So the broadband peaked at 400 nm in the Ni-implanted crystal is not due to the F-type color centers.

XPS results show that the implanted Ni ions are mainly in charge state of metallic  $\text{Ni}^0$  and probably in charge state of  $\text{Ni}^{2+}$  or  $\text{Ni}^{3+}$ . The HAADF STEM cross-sectional image proves the existence of metallic Ni nanoparticles with size 1 to 5 nm in diameter. As is well known,  $\text{Ni}^{2+}(3d^8)$  is optical active and often applied in laser devices, e.g.,  $\text{Ni}^{2+}:\text{MnF}_2$  crystals had been successfully used to obtain tuning laser

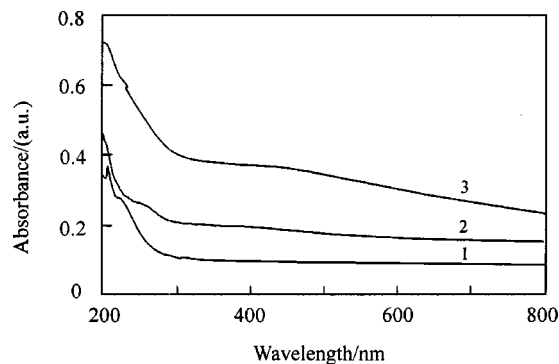


FIG. 4. Optical absorption spectra of as-grown, as-implanted and electron-irradiated  $\text{Al}_2\text{O}_3$  crystals. A broadband peaked at 400 nm appeared in the Ni-implanted sample. (1) as-grown (2) electron-irradiated, and (3) as-implanted.

peaked at 1.63  $\mu\text{m}$  in 1963.<sup>13</sup> Optical absorption spectrum of  $\text{Ni}^{2+}$  in silicate and silica glasses is known to be decomposed into three Gaussian components.<sup>14</sup> The positions are around 667, 526, and 455 nm, respectively, and vary in narrow limits with different  $\text{Ni}^{2+}$  ion concentration. The two high-frequency components are due to the transition  ${}^3A_{2g}(\text{F}) \rightarrow {}^3T_{1g}(\text{P})$  of  $\text{Ni}^{2+}$  in a distorted octahedral environment, and the other may be due to the spin-forbidden transition  ${}^3A_{2g}(\text{F}) \rightarrow {}^1E_g(\text{D})$  of  $\text{Ni}^{2+}$  in this octahedral site or to the transition  ${}^3T_1(\text{F}) \rightarrow {}^3T_1(\text{P})$  of  $\text{Ni}^{2+}$  in a tetrahedral coordination. In addition, the room-temperature absorption of  $\text{Ni}^{2+}$  in  $\text{BaLiF}_3$  for laser applications shows also three main broadbands peaking at 1180, 700, and 390 nm. And its luminescence spectra are three bands: 1.5  $\mu\text{m}$ , 740 nm, and 480 nm.<sup>15</sup> In our experiments, we did not detect any emission band in the as-implanted sample under a Xe lamp excitation wavelength of 250–430 nm in a spectrophotometer. Therefore, the broadband peaked at 400 nm in the as-implanted crystal is owing to Ni nanoparticles rather than color centers or  $\text{Ni}^{2+}$ , which may contribute to crystals turning gray.

In general, ion implantation techniques used to form nanocrystals may be categorized as follows:<sup>1,16–18</sup> (1) room temperature implantation followed by high temperature annealing; (2) room temperature implantation at dosage above the threshold dose for spontaneous nanocrystals formation; and (3) ion implantation at elevated temperatures. In this study, Ni nanoparticles formation by means of the second. At room temperature,  $1 \times 10^{17} \text{ cm}^{-2}$  exceeds the threshold dose, so the implanted Ni ions precipitate and form nanocrystals spontaneously. As is shown in Fig. 4, the Ni-implanted area is entirely amorphized. Ion implantation induced amorphization has been discussed in detail.<sup>19</sup> The degree of disorder depends upon the implantation parameters of ion dose, ion species, target temperature and orientation of the ion beam relative to crystallographic axes. The disorder increased faster with increasing dose for the *c*-axis orientation than the *a*-axis orientation. (0001) surfaces implanted sapphire with Fe ion become amorphous at a dose between  $1 \times 10^{17}$  and  $2 \times 10^{17} \text{ cm}^{-2}$ .<sup>20</sup>

It is conceivable that metallic nanocrystals are very active owing to its small size and high specific surface area. Optical properties of metallic nanoparticles embedded in a dielectric host are dominated by surface plasmon resonance (SPR) absorption.<sup>1</sup> The SPR absorption bands of Au and Ag nanoparticles in  $\text{SiO}_2$  are centered at 530 and 400–410 nm, respectively.<sup>4–5</sup> The CuS sample exhibits an absorption band peak at about 560 nm, characteristic of nanometric copper particles.<sup>21</sup> Ni nanoparticles embedded in  $\text{SiO}_2$  are known to give a SPR absorption of very low intensity, centered at about 350 nm.<sup>22</sup> Position, intensity, and width of the SPR absorption depend on the optical properties of both the metal species and the host matrix. Xu and Käll utilized extended the Mie theory to model the optical response of SPR of spherical metallic nanoparticles.<sup>23</sup> The model indicated that the SPR peak would shift towards low energy with increasing refractive index of surrounding medium. An alumina single crystal has a higher refractive index (1.76) than silica glass (1.52). Accordingly, the SPR peak of  $\text{Al}_2\text{O}_3$  (400 nm) has a redshift than that of  $\text{SiO}_2$  (350 nm). In addition, for the

smaller particle sizes, the plasmon band are relatively weak, broadened, and is shifted to higher energy due to quantum confinement.<sup>1</sup> In our experiments, the size of Ni nanoparticles ranges from 1 to 5 nm in diameter, which results in the broad and weak SPR absorption band. The optical absorption properties of metallic nanoparticles embedded in dielectric matrix materials due to surface plasma resonance can be used as optical filters and other optical components.

Metallic Ni nanoparticles, 1–5 nm in diameter, formed after 64 keV,  $1 \times 10^{17} \text{ cm}^{-2}$  Ni ion implantation at room temperature. Nanoparticles distributed from the surface to 30 nm below the surface were observed in a HAADF image. A HREM image indicated the Ni-implanted area had been entirely amorphized. A new broad absorption band centered at 400 nm appeared in the optical absorption spectrum of the as-implanted crystal, due to SPR of Ni nanoparticles. We did not find any emission band in the as-implanted sample under a Xe lamp excitation wavelength of 250–430 nm in a spectrophotometer.

This study was supported financially by the NSAF Joint Foundation of China No. 10376006 and by US Department of Energy under Grant No. DF-FG02-02ER46005.

- <sup>1</sup>A. Meldrum, R. F. Haglund, Jr., L. A. Boatner, and C. W. White, *Adv. Mater.* (Weinheim, Ger.) **13**, 1431 (2001).
- <sup>2</sup>G. W. Arnold, and J. A. Borders, *J. Appl. Phys.* **48**, 1488 (1977).
- <sup>3</sup>R. H. Magruder III, L. Yang, R. F. Haglund, Jr., C. W. White, L. Yang, R. Dorsinville, and R. R. Alfano, *Appl. Phys. Lett.* **62**, 1730 (1993).
- <sup>4</sup>Z. Liu, H. Li, X. Feng, S. Ren, H. Wang, Z. Liu, and B. Lu, *J. Appl. Phys.* **84**, 1913 (1998).
- <sup>5</sup>D. E. Hole, P. D. Townsend, J. D. Barton, L. C. Nistor, and J. Van Landuyt, *J. Non-Cryst. Solids* **180**, 266 (1995).
- <sup>6</sup>C. W. White, D. K. Thomas, D. K. Hensley, R. A. Zuhr, J. C. McCallum, A. Pogany, R. F. Haglund, R. H. Magruder, and L. Yang, *Nanostruct. Mater.* **3**, 447 (1993).
- <sup>7</sup>D. O. Henderson, R. Mu, Y. S. Yung, M. A. George, A. Burger, S. H. Morgan, C. W. White, R. A. Zuhr, and R. H. Magruder, *J. Vac. Sci. Technol. B* **13**, 1198 (1995).
- <sup>8</sup>E. Alves, C. MacHargue, R. C. Silva, C. Jesus, O. Conde, M. F. da Silva, and J. C. Soares, *Surf. Coat. Technol.* **128–129**, 434 (2000).
- <sup>9</sup>E. M. Hunt and J. M. Hampikian, *J. Mater. Sci.* **36**, 1963 (2001).
- <sup>10</sup>M. M. J. Treacy, A. Howie, and C. J. Wilson, *Philos. Mag. A* **38**, 569 (1978).
- <sup>11</sup>W. Chen, H. Tang, C. Shi, J. Deng, J. Shi, Y. Zhou, S. Xia, Y. Wang, and S. Yin, *Appl. Phys. Lett.* **67**, 317 (1995).
- <sup>12</sup>S. Choi and T. Takeuchi, *Phys. Rev. Lett.* **50**, 1474 (1983).
- <sup>13</sup>L. F. Johnson, R. E. Dietz, and H. J. Guggenheim, *Phys. Rev. Lett.* **11**, 318 (1963).
- <sup>14</sup>H. Keppeler and N. Bagdassarov, *Chem. Geol.* **158**, 105 (1999).
- <sup>15</sup>S. L. Baldochi, A. M. E. Santo, E. Martins, M. Duarte, M. M. F. Vieira, N. D. Vieira, Jr., and S. P. Morato, *J. Cryst. Growth* **166**, 375 (1996).
- <sup>16</sup>C. W. White, J. D. Budai, S. P. Withrow, J. G. Zhu, E. Sonder, R. A. Zuhr, A. Meldrum, D. M. Hembree, Jr., D. O. Henderson, and S. Praver, *Nucl. Instrum. Methods Phys. Res. B* **141**, 228 (1998).
- <sup>17</sup>D. Ila, E. K. Williams, R. L. Zimmerman, D. B. Poker, and D. K. Hensley, *Nucl. Instrum. Methods Phys. Res. B* **166–167**, 845 (2000).
- <sup>18</sup>S. M. Duvanov and A. G. Balogh, *Nucl. Instrum. Methods Phys. Res. B* **171**, 475 (2000).
- <sup>19</sup>C. J. McHargue, *Mater. Sci. Eng., A* **253**, 94 (1998).
- <sup>20</sup>S. X. Ren, C. J. Mchargue, L. F. Allard, Y. Chen, J. D. Hunn, B. N. Lucas, and R. K. Williams, *Microstructure of Irradiated Materials* (Materials Research Society, Pittsburgh, PA, 1995), p. 305.
- <sup>21</sup>E. Cattaruzza, G. Battaglin, R. Polloni, T. Cesca, F. Gonella, G. Mattei, C. Maurizio, P. Mazzoldi, F. D'Acapito, F. Zontone, and R. Bertonecello, *Nucl. Instrum. Methods Phys. Res. B* **148**, 1007 (1999).
- <sup>22</sup>T. Isobe, S. Y. Park, and R. A. Weeks, *J. Non-Cryst. Solids* **189**, 173 (1995).
- <sup>23</sup>H. X. Xu and M. Käll, *Sens. Actuators B* **87**, 244 (2002).